


Point-Defect Nature of the Ultraviolet Absorption Band in AlN

D. Alden,¹ J. S. Harris,¹ Z. Bryan,¹ J. N. Baker,¹ P. Reddy,¹ S. Mita,² G. Callsen,³ A. Hoffmann,³
D. L. Irving,¹ R. Collazo,¹ and Z. Sitar¹

¹*Department of Materials Science and Engineering, North Carolina State University,
Raleigh, North Carolina 27695, USA*

²*Adroit Materials, Inc., 2054 Kildaire Farm Road, Suite 205, Cary, North Carolina 27518, USA*

³*Institut für Festkörperphysik, Technische Universität Berlin,
Hardenbergstrasse 36, 10623 Berlin, Germany*

 (Received 11 January 2018; revised manuscript received 12 February 2018; published 24 May 2018)

We present an approach where point defects and defect complexes are identified using power-dependent photoluminescence excitation spectroscopy, impurity data from SIMS, and density-functional-theory (DFT)-based calculations accounting for the total charge balance in the crystal. Employing the capabilities of such an experimental computational approach, in this work, the ultraviolet-C absorption band at 4.7 eV, as well as the 2.7- and 3.9-eV luminescence bands in AlN single crystals grown via physical vapor transport (PVT) are studied in detail. Photoluminescence excitation spectroscopy measurements demonstrate the relationship between the defect luminescent bands centered at 3.9 and 2.7 eV to the commonly observed absorption band centered at 4.7 eV. Accordingly, the thermodynamic transition energy for the absorption band at 4.7 eV and the luminescence band at 3.9 eV is estimated at 4.2 eV, in agreement with the thermodynamic transition energy for the C_N^- point defect. Finally, the 2.7-eV PL band is the result of a donor-acceptor pair transition between the V_N and C_N point defects since nitrogen vacancies are predicted to be present in the crystal in concentrations similar to carbon-employing charge-balance-constrained DFT calculations. Power-dependent photoluminescence measurements reveal the presence of the deep donor state with a thermodynamic transition energy of 5.0 eV, which we hypothesize to be nitrogen vacancies in agreement with predictions based on theory. The charge state, concentration, and type of impurities in the crystal are calculated considering a fixed amount of impurities and using a DFT-based defect solver, which considers their respective formation energies and the total charge balance in the crystal. The presented results show that nitrogen vacancies are the most likely candidate for the deep donor state involved in the donor-acceptor pair transition with peak emission at 2.7 eV for the conditions relevant to PVT growth.

DOI: [10.1103/PhysRevApplied.9.054036](https://doi.org/10.1103/PhysRevApplied.9.054036)

I. INTRODUCTION

For nitride-based ultraviolet-C (UVC) optoelectronic devices, single-crystal AlN is the ideal substrate material. AlN substrates with average dislocation densities $<10^3 \text{ cm}^{-2}$ are available [1–3] and enable the growth of epitaxial layers of high-aluminum-content (Al,Ga)N thin films with unrivaled quality due to the low lattice mismatch and low dislocation density in the substrate [4–6]. Nevertheless, point defects in AlN single crystals lead to light absorption at energies lower than that of the 6.1-eV band-gap energy, which hinders the implementation of AlN substrates in applications where transparency is necessary. State-of-the-art AlN bulk crystals are grown via physical vapor transport (PVT) in inductively heated vertical reactors, where the N -polar surfaces of AlN single crystals are implemented as seeds [1–3]. In early studies, the measured below-band-gap absorption and luminescence bands have been attributed to oxygen [7,8]. Strassburg *et al.* [9] and Bickermann *et al.* [10], in separate studies, performed glow

discharge mass spectrometry analysis on various PVT-grown AlN single crystals and concluded that oxygen alone cannot explain the absorption and luminescent bands present in these crystals. Carbon impurities in concentrations similar to that of oxygen were consistently measured in the AlN single crystals, indicating that carbon must play a significant role in the optical properties of the crystals.

A particularly strong absorption band centered at 4.7 eV is measured in PVT-grown AlN single crystals. The presence of photoluminescence (PL) peaks at 2.7 and 3.9 eV has also been observed in samples displaying the strong absorption band at 4.7 eV [11–14]. The absorption band centered at 4.7 eV with an onset at 4.2 eV is observed only in AlN crystals, which contain carbon concentrations higher than or comparable to that of oxygen and/or silicon [11–15]. Hartmann *et al.* [2] determined that the oxygen-to-carbon concentration ratio needs to be equal to or larger than 3 in order to suppress the related absorption band. Additionally, the absorption coefficient at 4.7 eV decreases

with total sum concentration of carbon and oxygen for a given concentration ratio of the two [2,11]. These results clearly show that carbon impurities are present in PVT-grown AlN single crystals at significant concentrations and lead to the commonly observed absorption band at 4.7 eV. This is in contrast to the conclusions made by Slack *et al.* [8] where the increase of the absorption coefficient at 4.7 eV is attributed to an increase in oxygen-related defects [8]. In the latter study, however, no other impurities are considered, such as carbon, and the oxygen concentration measurements are limited to one sample. Collazo *et al.* [11] attribute this absorption band to the presence of negatively ionized carbon impurities which incorporate as substitutional nitrogen (C_N^-) [11]. This conclusion is based on the calculations of defect-formation energies as well as thermodynamic and optical transitions using density-functional theory (DFT), which are in agreement with absorption and PL spectra as well as secondary-ion mass spectroscopy (SIMS) measurements [11,14].

In this work, the UV absorption band at 4.7 eV and the luminescence bands at 2.7 and 3.9 eV are directly linked to the same defect state with a thermodynamic transition energy of 4.2 eV through photoluminescence excitation spectroscopy (PLE). Power-dependent PL measurements reveal the presence of an energy state within the band gap with a 5.0-eV thermodynamic transition energy, in agreement with the predicted energy state for the donor-acceptor pair (DAP) transition leading to the 2.7-eV luminescence band. Using these observations, an approach that combines all these observations with theoretical predictions arising from the implementation of charge and mass balance equations using DFT-derived formation energies is used to suggest the type and concentration of the point defects within these crystals.

II. EXPERIMENTAL DETAILS

The single-crystal AlN substrates studied in this work were obtained from AlN boules grown in a PVT-based process in a vertical rf-heated reactor [3]. A point-defect concentration of 2×10^{19} , 7×10^{18} , and $8 \times 10^{18} \text{ cm}^{-3}$ is measured for carbon, silicon, and oxygen, respectively, via SIMS. These are the typical impurity concentrations measured for UV-opaque crystals with absorption coefficients at 265 nm greater than 1000 cm^{-1} . The concentration of impurities in PVT-grown AlN single crystals and their relation to the prominent UVC absorption band has been studied in detail [2,13].

PL measurements are performed using an ArF excimer laser as an excitation light source (5-ns pulse width at an emission wavelength of 193 nm). The luminescence is directed onto a 0.75-m focal length Acton Series SP-2750 monochromator, where a 150 grooves/mm diffraction grating is used, and the intensity is recorded using a PIXIS-XO: 2KB CCD detector.

A 450-W XBO xenon short-arc lamp collimated by an elliptical mirror is used as an excitation source for the PLE spectroscopy. In order to ensure sufficient stray light reduction, the emission of this lamp is monochromatized by an additive double monochromator (0.225-cm focal length, 2400 grooves/mm, 250-nm blaze angle) before being focused onto the sample at an angle of 45° . The luminescence is collected by a second identical lens under an angle of 0° in order to suppress the excitation light in the detection beam path. Consequently, while the excitation double monochromator is scanned over the wavelength range of interest, the luminescence is monitored via a single monochromator (1-m focal length, 150 grooves/mm, 300-nm blaze angle) equipped with an UV-enhanced CCD. As a result, polychromatic PLE spectra can be recorded down to a wavelength of 200 nm. Here, great care must be taken in order to minimize stray light in the detection monochromator introduced by the excitation lamp, especially when the excitation source's wavelength and the detection wavelength approach each other (multiple reflections in the single monochromator introduced by the highly reflective surface of the CCD). Hence, we introduce two crossed linear polarizers (extinction ratio better than 1:2500 in the wavelength range of interest) into the excitation and detection beam paths in order to obtain pure PLE spectrum. Subsequently, all recorded PLE spectra are response corrected by monitoring the intensity of the excitation lamp.

For the absorption measurements, the samples are mechanically polished to a final thickness of $100 \mu\text{m}$, and an optical finish is obtained using $0.3\text{-}\mu\text{m}$ alumina slurry. A 150-W UV-enhanced Xe dc arc lamp is used as a broadband light source.

DFT calculations are performed using the Vienna *ab initio* simulation package 5.3 [16]. The hybrid exchange-correlation functional of Heyd *et al.* is used in the calculations in order to obtain a more realistic band gap [17,18]. This functional includes a fraction of the short-range exact Hartree-Fock exchange set to $\alpha = 0.32$, which results in an AlN band gap of 6.1 eV, consistent with our previous results. All calculations are performed in a 96-atom supercell with a $2 \times 2 \times 2$ k -point mesh and a 500-eV kinetic energy cutoff.

Defect-formation energies are calculated according to the standard grand canonical formalism [19,20]. The formation energy of a point defect in charge state q , X^q is given by

$$\Delta H_f(X^q) = [E_{\text{tot}}(X^q) + E_{\text{corr}}(X^q)] - E_{\text{tot}}(\text{bulk}) - \sum_i n_i \mu_i + q[E_{\text{VBM}} + E_F]. \quad (1)$$

Here, $E_{\text{tot}}(X^q)$ is the DFT energy of a supercell containing the defect X^q , and $E_{\text{tot}}(\text{bulk})$ is the DFT energy of the

corresponding bulk cell. $E_{\text{corr}}(X^q)$ is a finite-size correction for charged defect cells, which is obtained with a post-processing method based on that of Kumagai and Oba [21]. μ_i is the chemical potential of species i , and n_i is the number of atoms of species i exchanged between the bulk and a chemical reservoir in order to create the defect. The chemical potentials are a reflection of the environmental conditions during processing (e.g., Al-rich or N-rich conditions). E_{VBM} is the valence-band maximum (VBM), and E_F is the Fermi level relative to the VBM.

In this formalism, defect-formation energies are a function of the Fermi level, which is treated as a free parameter for the purpose of plotting the formation energies. Because defect concentrations are exponentially related to their formation energies, it is typical that only the lowest-energy charge state is plotted for a given defect at each Fermi level. For a given defect, the Fermi levels at which the charge state q (the slope of the line) changes are called thermodynamic transition levels and represent defect states within the band gap. Defect-formation energies can be accurate to within 0.1 eV, which also affects the accuracy of the predicted thermodynamic transition levels.

Defect concentrations may be obtained for a given set of environmental conditions (chemical potentials and/or impurity concentrations) by solving a charge neutrality expression involving the concentrations of defects, electrons, and holes in the system [14]. Charge neutrality is achieved by finding the Fermi level at which the sum of the ionized donors and holes is equal to the sum of the ionized acceptors and electrons. Here, defect concentrations are calculated after growth and quenching by assuming a near Al-rich environment and fixed impurity concentrations corresponding to the experimental values.

III. RESULTS AND DISCUSSION

The PL spectrum (black) overlapped with the absorption coefficient spectrum (red) is shown in Fig. 1. An absorption band centered at 4.7 eV is revealed with an absorption onset at 4.2 eV. The absorption coefficient plateaus at 4.5 eV until 4.8 eV, where it then decreases until 5.1 eV. For photon energies larger than 5.1 eV, the absorption coefficient increases again.

The PL spectrum in Fig. 1 shows two main luminescence bands centered at 3.9 and 2.7 eV. When fitting the asymmetric band centered at 2.7 eV, an overlapping lower-energy luminescence band centered at 2.5 eV is estimated [22]. An additional luminescent peak centered at 4.5 eV (lower in intensity) is also present. Through power-dependent PL measurements, the 4.5-eV luminescence band is more clearly revealed (Fig. 2). As the pulse peak power density is increased and defect states are saturated, the intensity of the PL band centered at 4.5 eV increases. The highest-energy edge of this band is estimated at 5.0 eV.

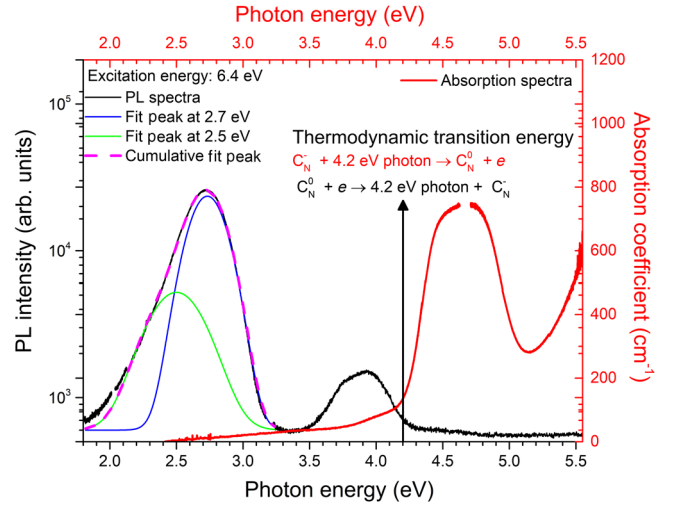


FIG. 1. PL spectrum (black) for above-band-gap energy excitation of an AlN single crystal overlapped with its absorption coefficient spectrum (red) for comparison. The asymmetric PL band with peak energy of 2.7 eV is fitted with two Gaussian functions in order to estimate the underlying independent luminescence centers.

This result indicates the presence of a midgap energy state with a 5.0-eV thermodynamic transition energy.

In the Franck-Condon approximation, it is assumed that the optoelectronic transition occurs in a short timescale when compared to the nuclear motion in the vicinity of the point defect. Therefore, the transition is assumed to occur at fixed nuclear coordinates [23]. Assuming the initial state is at equilibrium, from conservation of momentum, the probability of an optoelectronic transition will be proportional to the overlap between the zeroth quantum-number vibrational wave function in the initial state with the n th ($n = 0, 1, 2, 3, \dots$) quantum-number vibrational wave

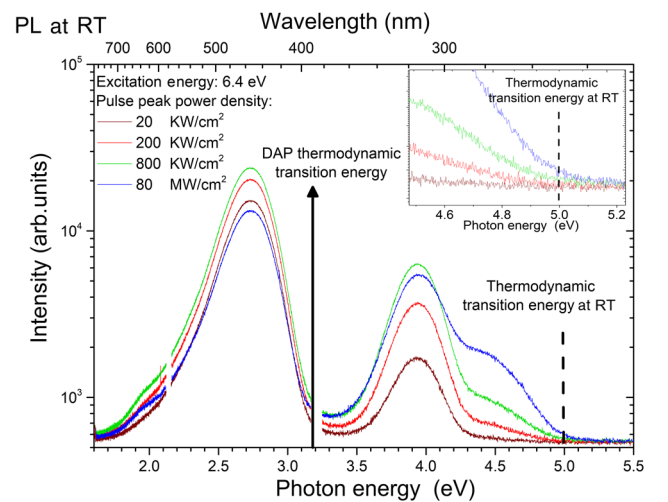


FIG. 2. Power-density-dependent PL measurements for above-band-gap energy excitation. As the power is increased, the luminescence band centered at 4.5 eV increases in intensity.

function in the final state of the point defect. More generally, Fermi's golden rule states that the transition probability P_{tran} is proportional to the square of the transition dipole moment, which under the Franck-Condon approximation can be separated into the electronic transition dipole moment μ_e and a nuclear term μ_{FC} , with

$$P_{\text{tran}} \sim |\mu_e|^2 \mu_{\text{FC}}. \quad (2)$$

In this work, we are interested in the effects that the nuclear term has on the shape of the absorption and photoluminescence spectra. For this reason, the electronic transition is assumed to be allowed, and μ_e is normalized and assumed to be independent of the coordinate position. The transition probability P_{tran} , which determines the shape of the luminescence spectrum from the zeroth vibrational state of the initial state into the n th vibrational state of the final state, can be described by the following equation [24]:

$$P_{\text{tran}}(\hbar\omega, T) = \sum_n w(T) |\langle \chi_{ne} | \chi_{0g} \rangle|^2 \delta(E_{\text{therm}} - n\hbar\omega_v - \hbar\omega_{\text{photon}}). \quad (3)$$

Here, $w(T)$ is the thermal occupation factor of the vibrational energy state, ω_v is the vibrational frequency, ω_{photon} is the photon frequency, E_{therm} is the thermodynamic transition energy, and $\langle \chi_{ne} | \chi_{0g} \rangle$ are the Franck-Condon overlap integrals of the vibrational wave functions.

From Eq. (3), the highest allowed photon energy for the radiative recombination [$n = 0$ in Eq. (3)] is equal to the thermodynamic transition energy of the point defect [25]. In analogy, for absorption, the minimum photon energy required to bring the point defect into an excited state (onset of absorption) is also equal to the thermodynamic transition energy. The vibrational wave-function overlap $\langle \chi_{ne} | \chi_{0g} \rangle$ between the initial and final ground states of a point defect is expected to decrease with increasing distance between their respective equilibrium coordinates in the crystal. This decrease in overlap leads to a reduced emission and

absorption probability at the thermodynamic transition energy. A representative configuration coordinate diagram is displayed in Fig. 3.

When analyzing the intersection of the absorption with the PL spectrum in Fig. 1, indeed, the estimated high-energy edge at 4.1 eV of the PL band centered at 3.9 eV matches the calculated thermodynamic transition energy of 4.2 eV for the $\text{C}_{\bar{\text{N}}}$ point defect as well as the onset of the absorption band centered at 4.7 eV. Despite these suggestive observations, it is not possible to make this conclusion based on the above-band-gap excitation PL spectrum and the measured absorption spectrum due to the large number of possible defects and their overlapping electro-optical transition energies. To precisely determine the electro-optical dynamics between the luminescence and absorption centers, PLE spectroscopy measurements are conducted.

In Fig. 4(a), a color-coded contour map with logarithmic intensity is shown. In this figure, the horizontal axis represents the detection energy of the sample's PL and ranges from 1.95 to 4.5 eV, while the vertical axis describes the energy of the excitation light source and ranges from 3.6 to 5.5 eV. The PLE spectra in Fig. 4(a) show the onset of the luminescence band centered at 3.9 eV at an excitation energy of 4.2 eV. This is in excellent agreement with the model where $\text{C}_{\bar{\text{N}}}$ is the point defect responsible for the UV absorption band as well as the luminescence band centered at 3.9 eV [11] and is further corroborated by Fig. 4(b), where a single spectrum is extracted from the contour map. The vertical blue and green lines in Fig. 4(a) correspond to the blue and green PLE curves in Fig. 4(b), while the horizontal black and gray lines in Fig. 4(a) correspond to the black and gray curves in Fig. 4(b) and represent the PL spectrum for a given excitation energy. Looking at the PLE spectrum with the detection energy fixed at 3.93 eV (blue line), an exponential increase in the intensity is observed when the excitation energy reaches 4.2 eV and peaks at 4.5 eV where it plateaus. Furthermore, the PL spectrum for an excitation energy of 4.5 eV (black line) shows that the high-energy edge of the PL band centered at 3.9 eV is 4.2 eV, which matches the onset of the PLE spectrum with 3.93-eV detection energy as expected under the Franck-Condon approximation as described previously. These results are direct evidence linking the 3.9-eV PL band and the 4.7-eV absorption band to a common defect with a thermodynamic transition energy of 4.2 eV.

The PLE measurements show that $\text{C}_{\bar{\text{N}}}$ is also involved in the radiative transition leading to the luminescence band centered at 2.7 eV which is evident from the PLE curve in Fig. 4(b) with fixed detection energy at 2.95 eV (light blue line), which shows an identical excitation channel to that of the 3.9-eV luminescence band. The detection energy of this PLE spectrum is purposely shifted from the peak emission at 2.7 to 2.95 eV in order to avoid any intensity originating from the overlapping luminescence sideband with peak emission at 2.5 eV, as is observed in the PLE spectrum with

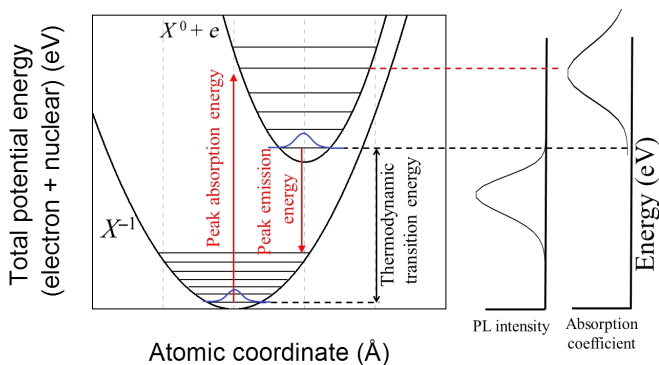


FIG. 3. Schematic illustrating the Franck-Condon energy shift for the absorption and photoluminescence arising from a shift in the configuration coordinate position of the potential minima for the initial and final states of the point defect.

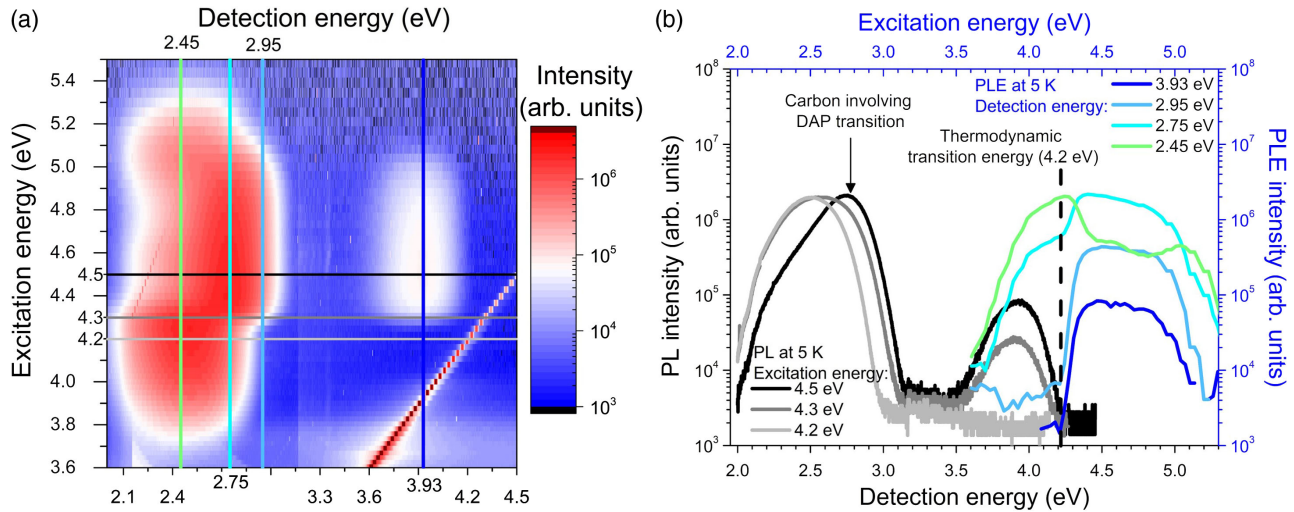


FIG. 4. (a) Color-coded logarithmic intensity 2D map photoluminescence excitation spectroscopy measurements of an AlN single crystal recorded at 5 K. The vertical lines correspond to PLE spectra for a fixed detection energy and are displayed as blue curves in (b). The horizontal lines in (a) correspond to PL spectra at fixed excitation energies and are displayed in (b) as black curves.

detection energy at 2.75 eV (cyan line). The PL band with peak energy at 2.5 eV has an onset excitation energy at 3.6 eV obtained from the PLE spectrum with detection energy at 2.45 eV [green curve in Fig. 4(b)]. These results clearly distinguish the origin of the PL band with peak energy at 2.7 eV from the PL band with peak energy at 2.5 eV, indicating that the 2.5-eV PL band is related to a thermodynamic transition with an energy of 3.6 eV [22] and was hypothesized to be related to Si in the donor-acceptor (DX) state and an acceptor (likely C_N) by Lamprecht *et al.* [22]. From the PL spectrum in Fig. 4(b) with 4.5-eV excitation energy (black line), the thermodynamic transition energy of the 2.7-eV luminescence band is estimated at 3.1 eV. Assuming the nature of this PL band is a DAP transition involving carbon, a deep donor state at 5.0 eV above the valence-band maximum is expected based on the thermodynamic energy level of the C_N^- acceptor state being at 1.9 eV above the VBM. This prediction of a donor state at 5.0 eV is in agreement with the power-dependent PL measurements, where a thermodynamic transition energy of 5.0 eV is estimated.

In order to establish a hypothesis for the nature of the deep donor point defect, a DFT quantitative model is built. In this model, it is necessary to consider the formation energy of all plausible point defects and defect complexes as well as charge balance conservation. The calculated formation energy for a few of the considered potential point defects and defect complexes are displayed in Fig. 5 as a function of the Fermi-level energy for near Al-rich growth conditions. In this work, a comprehensive array of defects is considered: native point defects, substitutional carbon, oxygen, and silicon in both Al and N lattice sites, and all first nearest-neighbor complexes including the latter mentioned point defects (i.e., $C_N - C_{Al}$, $C_N - O_{Al}$, $Si_{Al} - O_N$, $O_N - V_{Al}$, etc.). Relative to the Al reference state at the temperature of

interest (liquid Al), the Al chemical potential necessary to scale the formation energies for the different defects is given by the Gibbs relationship $\Delta\mu_{Al} = kT \ln(P_{Al}^{eq}/P_V^{Al})$. In this expression, P_{Al}^{eq} represents the Al equilibrium partial pressure above AlN, and P_V^{Al} is the corresponding vapor pressure above liquid Al at the temperature of interest. The partial vapor pressure of aluminum over AlN at 2100°C under

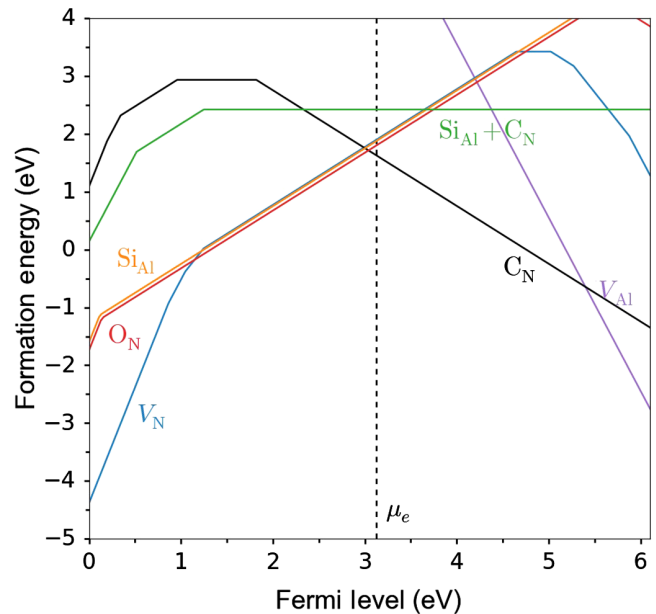


FIG. 5. Calculated formation energies for various likely point defects and defect complexes in PVT-grown AlN single crystals as a function of the Fermi level. Plotted -0.2 eV from the Al-rich growth condition with impurity chemical potentials determined assuming SIMS concentrations. The black dashed vertical line indicates the position of the equilibrium Fermi level after considering the charge balance equations at the growth temperature.

typical growth conditions is of the order of 50 mbar, and the Al vapor pressure over liquid aluminum is 120 mbar at the same temperature [26–28]. The difference in pressures corresponds to a relative displacement from the Al-rich extreme of -0.2 eV. Consequently, growth is expected to take place closer to the aluminum-rich conditions.

If the concentration of the main impurities in the crystal (carbon, oxygen, and silicon) is known, it is possible to estimate the chemical potential of the impurity self-consistently as part of the solution of the charge balance equations that include the formation energy for each charged defect present in the crystal. Such a method was recently implemented in complex oxides [29], and a detailed description of the methodology used to calculate the formation energies of the point defects and defect concentration will be published elsewhere. In Fig. 5, the formation energies of each impurity are plotted using the self-consistently determined impurity chemical potential.

The estimated defect concentrations are listed in Table I based on the SIMS measurements described in Sec. II and the previous chemical potential discussions. Only point defects in concentrations above $1 \times 10^{17} \text{ cm}^{-3}$ are listed in the table since lower concentrations are expected to contribute relatively insignificantly to the observed absorption band and related processes.

The calculated results indicate that in addition to oxygen and silicon, one of the main compensators for carbon point defects are nitrogen vacancies, consistent with the conclusions made by Gaddy *et al.* [14], which attributed the 2.7-eV luminescence to a DAP transition involving carbon and a nitrogen vacancy. This identification of 2.7 eV luminescence was based on DFT calculations that show a relatively low formation energy of the nitrogen vacancy compared to other impurities and its charge-compensating nature to the ionized carbon impurity [14].

The calculated thermodynamic transitions for the tabulated defects are presented as a diagram in Fig. 6. From the diagram, it is clear that the only band-to-defect transition with an energy difference close to 4.2 eV is the transition involving C_N^- to C_N^0 and the conduction-band minimum. Finally, in hydride vapor phase epitaxy (HVPE) grown AlN, by changing the C concentration, the absorption at 4.7 eV and luminescence at 2.7 and 3.9 eV reduce with a reduction in C, in agreement with our conclusions [11].

TABLE I. The calculated point-defect concentrations are displayed for point defects in concentrations above $1 \times 10^{17} \text{ cm}^{-3}$. The calculations take into consideration a fixed amount of carbon, oxygen, and silicon as measured by SIMS, a growth temperature of 2100°C, and utilize the methodology described in the text.

	C_N	V_N	O_N	Si_{Al}	$Si_{Al} - C_N$
Defect concentration ($\times 10^{19}/\text{cm}^3$)	1.9	0.5	0.8	0.6	0.1

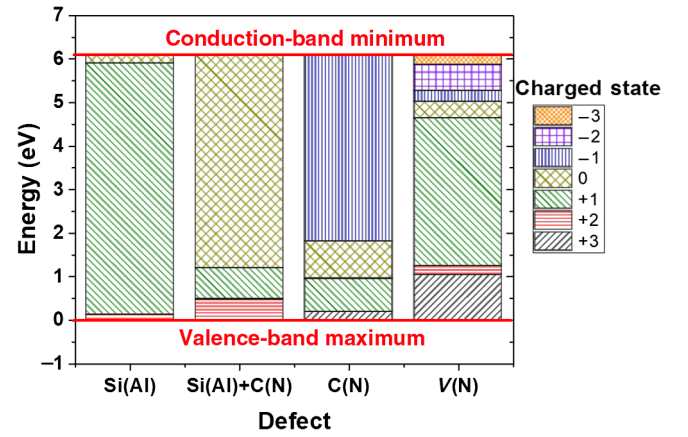


FIG. 6. Schematic displaying the thermodynamic transition energy states for the respective point defects as horizontal lines referenced to the valence-band maximum. The shaded regions indicate the charged state of the defect as a function of Fermi energy (y axis).

Further supporting the DAP hypothesis, the photoluminescence decay for the 2.7-eV peak measured by Lamprecht *et al.* [22] shows an initial fast decay followed by a slower decay indicative of a distribution in wave-function overlap, i.e., distribution of $V_N - C_N$ distances forming the donor-acceptor pair.

In addition, the diagram in Fig. 6 indicates three thermodynamic transition levels close to the measured 5.0-eV level that leads to the 2.7-eV DAP emission band. All three are associated with the nitrogen vacancy: the donor level at 4.7 eV, the acceptor level at 5.0 eV, and the doubly ionized acceptor level at 5.3 eV. From this, we establish the hypothesis that the observed 5.0-eV transition level corresponds to the V_N donor +1 charged state. Nevertheless, we do not see the close agreement between the predicted V_N donor level (4.7 eV) and the optical measurements (5.0 eV) that we see for the carbon acceptor level. The difference (close to the accuracy of our methods) can be attributed to many factors. Finite-size effects due to the small supercell used for the defect calculations limit the accuracy of DFT defect energies to the order of approximately 0.1 eV. Vacancies are surrounded by undercoordinated atoms, which tend to be freer to relax than the atoms neighboring the impurity defects. Nitrogen-vacancy donors exhibit large geometry changes between different ionized donor states and have large Franck-Condon shifts in the excitation spectra. A large coordinate shift may result in negligible or no vibrational overlap of the zeroth-order vibrational modes of the ground state and the excited state, which will apparently slightly shift toward higher energies the turn-on measured experimentally. The open geometry of the vacancy may facilitate the formation of several local minima (akin to DX centers for substitutional defects), which, in turn, influences the prediction of the thermodynamic transition level via a change in defect-formation energies. Ultimately, these issues need to be explored for

the DFT results to be accurate below 0.3 eV, but the qualitative position of the states predicted in Fig. 6 will not change. Of all the defects that are predicted to occur in significant concentrations, only the nitrogen vacancy has states in the vicinity of the turn-on measured experimentally within reasonable accuracy. It has to be noted that V_{Al} is invoked to explain the 2.7-eV emission [30] and is unlikely due to high formation energy. Although V_{Al} complexes with O are energetically favorable [30] and have transitions similar to C_{N} and may be relevant in AlN epitaxy, in PVT-grown AlN substrates, the C_{N} is the dominant impurity, as seen from SIMS (Table I).

The model further predicts that silicon on an aluminum site (Si_{Al}), oxygen on a nitrogen site (O_{N}), and a complex between carbon on a nitrogen site and silicon on an aluminum site ($\text{Si}_{\text{Al}} - C_{\text{N}}$) are also present in concentrations above 10^{17} cm^{-3} . Any optical transitions involving Si_{Al} or related to any possible transitions between the donor O_{N} and acceptor C_{N} are too high in energy and cannot explain the experimentally observed PL and PLE spectra.

IV. CONCLUSIONS

In this work, the luminescent bands at 3.9 and 2.7 eV are directly related to the 4.7-eV absorption band. The thermodynamic transition energy for the absorption band is estimated at 4.2 eV, in agreement with the thermodynamic transition energy for the C_{N}^- point defect. Nitrogen vacancies are predicted to be present in the crystal in concentrations similar to carbon. The calculated thermodynamic transition for V_{N} in the donor +1 charge state is 4.7 eV, thus, supporting the present hypothesis that this point defect is responsible for the observed thermodynamic transition at 5 eV for above-band-gap excitation. Furthermore, the identification of V_{N} as responsible for thermodynamic transition at 5 eV further supports the hypothesis that the 2.7-eV PL band is the result of a donor-acceptor pair transition between the V_{N} and C_{N} point defects. These conclusions help demonstrate the capabilities of such experimental computational approaches in which the development of the formation energy databases of all plausible point defects help in the development of quantitative models. These models can then be used to predict the influence of a variety of point defects within technologically important semiconductor systems. In conjunction with complementary optical characterization techniques, the possibility of establishing the role of a variety of point defects in determining the properties of different materials may be possible.

ACKNOWLEDGMENTS

The authors acknowledge partial financial support from the National Science Foundation (Grants No. ECCS-1508854, No. ECCS-1610992, and No. ECCS-1653383), Army Research Office (ARO) (Grants No. W911NF-15-2-0068 and No. W911NF-16-C-0101), and Air Force Office

of Scientific Research (AFOSR) (Grants No. FA9550-14-1-0264 and No. FA9550-17-1-0225). D. A. acknowledges CONACYT-Mexico for their financial support. This research uses the resources of the National Energy Research Scientific Computing Center, a Department of Energy, Office of Science User Facility supported by the Office of Science of the U.S. Department of Energy under Contract No. DE-AC02-05CH11231.

- [1] P. Lu, R. Collazo, R. F. Dalmau, G. Durkaya, N. Dietz, B. Raghathamachar, M. Dudley, and Z. Sitar, Seeded growth of AlN bulk crystals in *m*- and *c*-orientation, *J. Cryst. Growth* **312**, 58 (2009).
- [2] C. Hartmann, J. Wollweber, S. Sintonen, A. Dittmar, L. Kirste, S. Kollowa, K. Irmscher, and M. Bickermann, Preparation of deep UV transparent AlN substrates with high structural perfection for optoelectronic devices, *Cryst. Eng. Commun.* **18**, 3488 (2016).
- [3] Z. G. Herro, D. Zhuang, R. Schlessler, R. Collazo, and Z. Sitar, Seeded growth of AlN on N- and Al-polar AlN seeds by physical vapor transport, *J. Cryst. Growth* **286**, 205 (2006).
- [4] Z. Bryan, I. Bryan, J. Xie, S. Mita, Z. Sitar, and R. Collazo, High internal quantum efficiency in AlGaN multiple quantum wells grown on bulk AlN substrates, *Appl. Phys. Lett.* **106**, 142107 (2015).
- [5] I. Bryan, Z. Bryan, S. Mita, A. Rice, L. Hussey, C. Shelton, J. Tweedie, J.-P. Maria, R. Collazo, and Z. Sitar, The role of surface kinetics on composition and quality of AlGaN, *J. Cryst. Growth* **451**, 65 (2016).
- [6] R. Dalmau, B. Moody, R. Schlessler, S. Mita, J. Xie, M. Feneberg, B. Neuschl, K. Thonke, R. Collazo, A. Rice *et al.*, Growth and characterization of AlN and AlGaN epitaxial films on AlN single crystal substrates, *ECS Trans.* **33**, 43 (2010).
- [7] J. Pastrňák and L. Roskocova, Optical absorption edge of AlN single crystals, *Phys. Status Solidi B* **26**, 591 (1968).
- [8] G. A. Slack, L. J. Schowalter, D. Morelli, and J. A. Freitas, Jr., Some effects of oxygen impurities on AlN and GaN, *J. Cryst. Growth* **246**, 287 (2002).
- [9] M. Strassburg, J. Senawiratne, N. Dietz, U. Haboek, A. Hoffmann, V. Noveski, R. Dalmau, R. Schlessler, and Z. Sitar, The growth and optical properties of large, high-quality AlN single crystals, *J. Appl. Phys.* **96**, 5870 (2004).
- [10] M. Bickermann, B. M. Epelbaum, and A. Winnacker, Characterization of bulk AlN with low oxygen content, *J. Cryst. Growth* **269**, 432 (2004).
- [11] R. Collazo, J. Xie, B. E. Gaddy, Z. Bryan, R. Kirste, M. Hoffmann, R. Dalmau, B. Moody, Y. Kumagai, T. Nagashima, Y. Kubota, T. Kinoshita, A. Koukitu, D. L. Irving, and Z. Sitar, On the origin of the 265 nm absorption band in AlN bulk crystals, *Appl. Phys. Lett.* **100**, 191914 (2012).
- [12] M. Bickermann, B. M. Epelbaum, O. Filip, B. Tautz, P. Heimann, and A. Winnacker, Faceting in AlN bulk crystal growth and its impact on optical properties of the crystals, *Phys. Status Solidi C* **9**, 449 (2012).
- [13] K. Irmscher, C. Hartmann, C. Gugushev, M. Pietsch, J. Wollweber, and M. Bickermann, Identification of a

- tri-carbon defect and its relation to the ultraviolet absorption in aluminum nitride, *J. Appl. Phys.* **114**, 123505 (2013).
- [14] B. E. Gaddy, Z. Bryan, I. Bryan, R. Kirste, J. Xie, R. Dalmau, B. Moody, Y. Kumagai, T. Nagashima, Y. Kubota, T. Kinoshita, A. Koukitu, Z. Sitar, R. Collazo, and D. L. Irving, Vacancy compensation and related donor-acceptor pair recombination in bulk AlN, *Appl. Phys. Lett.* **103**, 161901 (2013).
- [15] P. Lu, R. Collazo, R. F. Dalmau, G. Durkaya, N. Dietz, and Z. Sitar, Different optical absorption edges in AlN bulk crystals grown in *m*- and *c*-orientations, *Appl. Phys. Lett.* **93**, 131922 (2008).
- [16] G. Kresse and J. Furthmüller, Efficient iterative schemes for *ab initio* total-energy calculations using a plane-wave basis set, *Phys. Rev. B* **54**, 11169 (1996).
- [17] J. Heyd, G. E. Scuseria, and M. Ernzerhof, Hybrid functionals based on a screened Coulomb potential, *J. Chem. Phys.* **118**, 8207 (2003).
- [18] J. Heyd, G. E. Scuseria, and M. Ernzerhof, Hybrid functionals based on a screened Coulomb potential, *J. Chem. Phys.* **118**, 8207 (2003); Erratum “Hybrid functionals based on a screened Coulomb potential”, *J. Chem. Phys.* **124**, 219906(E) (2006).
- [19] C. G. V. de Walle and J. Neugebauer, First-principles calculations for defects and impurities: Applications to III-nitrides, *J. Appl. Phys.* **95**, 3851 (2004).
- [20] C. Freysoldt, B. Grabowski, T. Hickel, J. Neugebauer, G. Kresse, A. Janotti, and C. G. Van de Walle, First-principles calculations for point defects in solids, *Rev. Mod. Phys.* **86**, 253 (2014).
- [21] Y. Kumagai and F. Oba, Electrostatics-based finite-size corrections for first-principles point defect calculations, *Phys. Rev. B* **89**, 195205 (2014).
- [22] M. Lamprecht, C. Grund, B. Neuschl, K. Thonke, Z. Bryan, R. Collazo, and Z. Sitar, Very slow decay of a defect related emission band at 2.4 eV in AlN: Signatures of the Si related shallow DX state, *J. Appl. Phys.* **119**, 155701 (2016).
- [23] E. Condon, A theory of intensity distribution in band systems, *Phys. Rev.* **28**, 1182 (1926).
- [24] A. Alkauskas, M. D. McCluskey, and C. G. Van de Walle, Tutorial: Defects in semiconductors—Combining experiment and theory, *J. Appl. Phys.* **119**, 181101 (2016).
- [25] A. E. Hughes, Zero-phonon transitions and vibrational structure, *J. Phys. (Paris), Colloq.* **28**, 55 (1967).
- [26] B. M. Epelbaum, M. Bickermann, and A. Winnacker, Seeded PVT growth of aluminum nitride on silicon carbide, *Mater. Sci. Forum* **433–436**, 983 (2003).
- [27] C. B. Alcock, V. P. Itkin, and M. K. Horrigan, Vapour pressure equations for the metallic elements: 298–2500 K, *Can Metall. Q.* **23**, 309 (1984).
- [28] V. Noveski, R. Schlessler, S. Mahajan, S. Beaudoin, and Z. Sitar, Mass transfer in AlN crystal growth at high temperatures, *J. Cryst. Growth* **264**, 369 (2004).
- [29] J. N. Baker, P. C. Bowes, D. M. Long, A. Moballegh, J. S. Harris, E. C. Dickey, and D. L. Irving, Defect mechanisms of coloration in Fe-doped SrTiO₃ from first principles, *Appl. Phys. Lett.* **110**, 122903 (2017).
- [30] Q. Yan, A. Janotti, M. Scheffler, and C. G. Van de Walle, Origins of optical absorption and emission lines in AlN, *Appl. Phys. Lett.* **105**, 111104 (2014).